Scientific Research Publishing

Computational Water, Energy, and Environmental Engineering, 2025, 14(4), 151-177
https://www.scirp.org/journal/cweee
ISSN Online: 2168-1570
ISSN Print: 2168-1562

Application of OpenOil in Modeling a Shipwreck Oil Spill: The Tobago Case

Vassilios Papaioannou*, Christos G. E. Anagnostopoulos, Anastasia Moumtzidou, Ilias Gialampoukidis, Stefanos Vrochidis, Ioannis Kompatsiaris

Information Technologies Institute, Centre for Research and Technology Hellas, Thessaloniki, Greece
Email: *vaspapa@iti.gr, anagn_c@iti.gr, moumtzid@iti.gr, heliasgj@iti.gr, stefanos@iti.gr, ikom@iti.gr

How to cite this paper: Papaioannou, V., Anagnostopoulos, C.G.E., Moumtzidou, A., Gialampoukidis, I., Vrochidis, S. and Kompatsiaris, I. (2025) Application of OpenOil in Modeling a Shipwreck Oil Spill: The Tobago Case. *Computational Water, Energy, and Environmental Engineering*, **14**, 151-177.
https://doi.org/10.4236/cweee.2025.144008

Received: August 19, 2025
Accepted: October 6, 2025
Published: October 9, 2025

Abstract

In February 2024, a shipwreck off Tobago caused a significant surface oil spill, highlighting the need for accurate modeling tools to support emergency response. This study applies the OpenOil module of the OpenDrift framework to simulate oil dispersion from this event, emphasizing the unique characteristics of shipwreck-origin continuous spills. The model incorporates three-dimensional ocean current data from the Copernicus Marine Environment Monitoring Service (CMEMS), along with wind and wave forcing, to simulate surface drift and weathering under tropical conditions. Validation against satellite imagery (Sentinel-1 and Sentinel-2) and *in-situ* observations was performed using the Success Rate (SR), Centroid Displacement Index (CI), and Centroid Skill Score (CSS). OpenOil effectively reproduced observed spill trajectories, with CSS values between 0.89 and 0.98. Model sensitivity was primarily influenced by wind conditions and oil properties. These findings demonstrate OpenOil's utility in simulating complex spill scenarios and underscore the need for scenario-specific calibration, improved environmental forcing, and expanded satellite-based validation for future response efforts.

Keywords

Continuous Discharge, Lagrangian Particle Tracking, Oil Spill Modeling, Oil Weathering, OpenOil, Satellite Validation, Shipwreck Oil Spill, Tropical Marine Environment

1. Introduction

Oil spills represent one of the most significant and persistent environmental challenges of the modern industrial era, posing severe threats to marine ecosystems, coastal communities, and global biodiversity [1]. These incidents occur when pe-

troleum hydrocarbons are accidentally or intentionally released into marine or terrestrial environments, creating pollution scenarios that can persist for decades [2]. Beyond visible damage, oil spills affect food webs, disrupt reproductive cycles of marine organisms, and cause long-term habitat degradation that influences ecosystem dynamics for years [3] [4]. Recent research in 2024 has further shown that oil spills profoundly impact microscopic seawater bacteria critical to ecosystem functioning, opening new avenues for improved cleanup processes [3].

From a socioeconomic perspective, oil spills impose substantial costs on affected communities through losses to fisheries, tourism, and coastal industries, while cleanup and restoration can cost billions of dollars and take years to complete [5]. For example, in fiscal year 2023 the NOAA Emergency Response Division supported the removal or mitigation of over 4795 pollution sources from U.S. coasts and oceans, including 95 vessels in Maui, underscoring the ongoing scale of marine pollution response efforts [6].

Maritime oil spills from shipping activities remain a major category of marine pollution, with tanker accidents historically responsible for some of the most catastrophic environmental disasters [5]. According to the International Tanker Owners Pollution Federation (ITOPF), ten tanker spills exceeding seven tonnes were reported in both 2023 and 2024, including six large spills (>700 tonnes) in 2024 alone. The total volume lost to the environment in 2024 was approximately 10,000 tonnes—higher than the previous year but still a fraction of the vast amounts transported annually by sea [5]. Although the decade average of 7.4 tanker spills per year reflects major reductions compared to earlier decades, each incident continues to pose substantial risks [5]. However, challenges remain in data accuracy, with a 2023 IMO study revealing a 20% discrepancy in spill reporting between countries with strict and loose regulations [5].

Geographically, oil spill distribution mirrors global shipping patterns, with higher rates in heavily trafficked corridors such as the English Channel, Mediterranean Sea, Persian Gulf, and approaches to major ports [7]. The Eastern Mediterranean, in particular, is highly vulnerable due to its strategic location between Europe, Asia, and Africa [8]. Contributing factors include mechanical failures, human error, adverse weather, collisions, and inadequate vessel maintenance [9].

Given these risks, accurate prediction of spill behavior is vital. Computational modeling has become a cornerstone of both response planning and scientific investigation. OpenOil, developed within the OpenDrift Lagrangian modeling system, provides a sophisticated framework for simulating oil spill transport, fate, and weathering processes [10]. Incorporating algorithms for entrainment, vertical mixing, resurfacing, and emulsification, and coupled with real-time meteorological and oceanographic data from systems such as Copernicus Marine Environment Monitoring [11], OpenOil enables researchers and responders to forecast oil movement under varying conditions [12].

This study applies the OpenOil module to simulate the transport and fate of oil from the 2024 Tobago spill, caused by a vessel wreck near the island's southern

coast [13]. The incident released significant oil along more than 25 km of coastline, threatening coral reefs and mangroves. Satellite observations from the European Space Agency [14] documented slicks spreading into the Caribbean Sea under the influence of currents and winds. Given Tobago's reliance on tourism and fisheries, the ecological and economic impacts were considerable [15] [16]. Complex oceanographic conditions, including variable currents and eddies, made predicting oil dispersal particularly challenging, highlighting the need for robust modeling tools [17].

The Tobago spill—characterized by continuous release from a shipwreck, delayed detection, and interaction with dynamic Caribbean circulation—provides a unique case study for testing oil spill modeling in complex marine environments with limited monitoring capacity. By integrating in situ observations with high-resolution Sentinel-1 (radar) and Sentinel-2 (optical) satellite imagery, this research evaluates OpenOil's ability to reproduce the observed spill evolution and improve predictive accuracy in sensitive ecosystems [18].

Accordingly, this study addresses the following questions:

- *How accurately can OpenOil simulate the transport and fate of oil from a shipwreck-origin spill, as exemplified by the Tobago case*?
- *To what extent can the OpenOil module effectively model a continuous oil spill, and what are its limitations and validation performance based on key metrics*?

2. Methodology

The methodology outlines the framework for modeling oil transport and dispersion, starting with an overview of the OpenOil model and its configuration. It then covers the key physical properties and equations governing horizontal and vertical transport. Next, the Tobago area simulation setup is described, followed by satellite imagery acquisition and preprocessing for model validation. Finally, the performance metrics used to evaluate the model's predictions are presented.

2.1. OpenOil Model and Its Requirements

1) OpenOil model: This study uses OpenDrift's OpenOil module to simulate the 2024 Tobago oil spill's transport and weathering. OpenOil models oil as individual particles (Lagrangian elements) with properties like mass, viscosity, and density, enabling detailed tracking of oil behavior under Tobago's conditions. Particle movement is driven by ocean currents, wind, Stokes drift, and random walk diffusion. The model includes physical processes such as wave entrainment [19], turbulence-driven mixing [20], buoyancy-driven resurfacing [21], and emulsification [22]. Resurfacing depends on droplet size and density, with sinking velocity based on Stokes Law, making droplet size distribution critical [23]. Oil properties come from the ADIOS database, covering nearly 1000 oil types worldwide [24].

2) Wind Data: Wind data were obtained from the Global Ocean Hourly Sea Surface Wind and Stress product, offering hourly wind and stress fields at 0.125˚

resolution. This dataset combines scatterometer data from Metop-B and Metop-C ASCAT with ECMWF model outputs, using temporally-averaged difference fields to correct model biases. It also includes divergence, curl, bias corrections, and variance measures [25]. Linear interpolation refined the data to 0.0045˚, but this higher resolution had minimal impact on oil particle movement while greatly increasing computational cost.

3) Hydrodynamic Data: The Operational Mercator Global Ocean Analysis and Forecast System provides daily-updated, 10-day 3D global ocean forecasts at 1/12˚ resolution. It aggregates data into a two-year sliding window, offering daily and monthly averages of temperature, salinity, currents, sea level, mixed layer depth, and ice conditions from surface to 5500 m depth across 50 vertical levels. Hourly surface data for sea level, temperature, and currents are also included. The data use a regular longitude/latitude projection. A specialized dataset, SMOC, merges surface currents with wave and tidal drift information [26].

4) Wave Data: The Météo-France global ocean wave forecast system provides daily analyses and 10-day forecasts of sea surface waves at 1/12˚ resolution. It delivers 3-hourly fields for wave parameters like significant wave height, period, direction, and Stokes drift, including partitions for wind waves and primary/secondary swells. Based on the MFWAM third-generation model using ECWAM-IFS-38R2 code, it incorporates dissipation and bathymetry from ETOPO2/NOAA. The irregular grid spacing decreases near the poles, with ~1/10˚ spacing at the equator. Driven by 6-hourly ECMWF wind analyses and 3-hourly forecasts, the wave spectrum is discretized into 24 directions and 30 frequency bands (0.035 - 0.58 Hz). Altimeter data assimilation occurs every 6 hours. Analyses run four times daily, starting at 00:00 UTC [27].

2.2. Physical Properties and Governing Equations

The simulations incorporate key physical processes affecting oil transport: 1) horizontal transport driven by currents, Stokes drift, and wind drift; and 2) vertical transport and mixing, including wave breaking, buoyancy-driven resurfacing, and turbulence-driven vertical movement.

2.2.1. Horizontal Transport

Oil particles move horizontally due to advection by currents, wind, and waves. Whether submerged or at the surface, they follow ambient currents and experience wind drift, typically about 1% - 6% of surface wind speed (averaging 3%). They are also affected by surface Stokes drift, modeled using the Phillips spectrum [28].

2.2.2. Vertical Transport

1) Wave entrainment: Wave entrainment refers to the process by which particles in the water are moved during stormy conditions and when waves break in the open sea. The mixing of oil near the surface in open seas is largely influenced by the energy from breaking waves [29]. To understand wave entrainment more

thoroughly, several factors are considered, such as the thickness, density, and viscosity of the oil, the oil-water surface tension, water density, gravity, the energy available from breaking waves to lift the oil, and the extent of the sea surface affected by breaking waves [19]. The rate of oil entrainment, Q, is described using two dimensionless numbers: Weber (We) and Ohnesorge (Oh). The equation for entrainment is given by:

$$Q = Q_0 F_{bw} \tag{1}$$

- where F_{bw} represents the fraction of the sea surface with breaking waves, and Q_0 is the dimensionless vertical oil flux from the sea surface into the water column, calculated using Equation (2):

$$Q_0 = aWe^b Oh^c \tag{2}$$

- where: $a = 4.604 \times 10^{-10}$, $b = 1.805$, and $c = -1.023$ according to [30]. Substituting these values into Equation 1, we get:

$$Q = 4.604 \times 10^{-10} We^{1.805} Oh^{-1.023} F_{bw} \tag{3}$$

- where: The F_{bw} factor is related to wind speed and wave period (the time between waves), based on [31], and is calculated as:

$$F_{bw} = \begin{cases} a_{bw} \dfrac{U_{10m} - U_o}{T_p}, & \text{if } U_{10m} > U_o \\ 0, & \text{if } U_{10m} \le U_o \end{cases} \tag{4}$$

- where: a_{bw} = 0.032 s/m (constant), U_{10m} is the wind speed at 10 meters above sea level, U_o is the minimum wind speed that starts wave breaking (considered equal to 5 m/s), and T_p is the significant wave period taken from the wave data.

The Weber number (We) helps determine how much inertial forces and oil-water surface tension play a role [31]. It is calculated as:

$$We = \frac{\rho_{sw} g H_s d_o}{\sigma_{ow}} \tag{5}$$

- where: ρ_{sw} is the seawater density (1028 kg/m^3), g is gravity (9.81 m/s^2), H_s is the significant wave height (taken from wave data), σ_{ow} is the oil-water surface tension (0.030126 mN/m for oil type Generic Light Crude), d_o is the Rayleigh-Taylor instability maximum diameter [31], given by:

$$d_o = 4\sqrt{\frac{\sigma_{ow}}{g\left(\rho_{sw} - \rho_{oil}\right)}} \tag{6}$$

- where: ρ_{oil} is the oil density (854.2 kg/m^3 for Generic Light Crude).

The Ohnesorge number (Oh) describes the balance between viscous forces and inertial or surface tension forces [31]. It is calculated using the oil's dynamic viscosity (μ_{oil} = 9.02 cPoise for Generic Light Crude), the oil density, the oil-water surface tension, and the Rayleigh-Taylor instability diameter:

$$Oh = \frac{\mu_{oil}}{\sqrt{\rho_{oil} \sigma_{ow} d_o}} \tag{7}$$

2) Oil resurfacing: Oil droplets in the water can rise back to the surface due to buoyancy, resulting in either resurfaced or submerged droplets depending on their size and density difference relative to the surrounding water [31]. The rate at which droplets rise is governed by their radius and the density contrast between oil and seawater. According to Tkalich and Chan [21], different formulas apply depending on droplet size: small droplets follow Stokes' law, while larger droplets are calculated using Reynolds' law. The vertical terminal velocity w is given by:

$$w(r)=\begin{cases}\sqrt{\dfrac{16}{3}g(1-\rho)r}, & \text{if } Re>50\\ \dfrac{2g(1-\rho)}{9v_{sw}}r^2, & \text{if } Re\le 50\end{cases} \tag{8}$$

- where: r is the droplet radius, $\rho=\rho_{oil}/\rho_{sw}$, v_{sw} is the kinematic water viscosity (=6.865 × 10^{-5} m^2/s) and $Re=2rw(r)/v_{sw}$ is the droplet Reynolds number.

Typical rise velocities vary greatly with droplet size and density. For example, a droplet with a diameter of 0.01 mm and density 900 kg/m^3 may rise at around 1 cm per hour, while a 0.5 mm droplet can ascend at up to 30 meters per hour [31]. Liu *et al.* [32] further reported that a 4 mm droplet with a density of 870 kg/m^3 can achieve a rise speed as high as 0.095 m/s.

3) Oil droplet distribution: When an oil droplet is released during a subsea blowout, it begins a slow ascent toward the surface. At such depths, droplet sizes vary considerably—ranging from as small as 0.1 mm (100 μm) to as large as 0.5 mm (500 μm) [33]. The rate at which these droplets rise is strongly influenced by their size: larger droplets ascend more rapidly due to greater buoyancy, while smaller droplets tend to remain suspended and are more readily transported by deep-sea currents. Research by Johansen *et al.* [34] and Li *et al.* [19] indicates that the distribution of oil droplet sizes is best described by a lognormal distribution. In this framework, the volume-based median droplet diameter (D_{50}^V) serves as a key parameter to characterize the size spectrum. According to Li *et al.* [19], D_{50}^V can be calculated using the following equation:

$$D_{50}^V=d_o r_e(1+10Oh)^p We^q \tag{9}$$

- where: $r_e=1.791$, $p=0.46$, and $q=-0.518$ are empirical coefficients [19].

The size distribution follows a lognormal distribution, where the probability density function (*PDF*) is given by:

$$PDF=\frac{1}{ds\sqrt{2\pi}}\exp\left(-\frac{\left(\ln d-\ln D_{50}^V\right)^2}{2s^2}\right) \tag{10}$$

- where: $s=0.38\pm0.05$ is the standard deviation of the distribution [31].

Finally, the volume size distribution, as described by Delvigne and Sweeney [35], is:

$$V(d)=d^{-0.7}, d\in[d_{\min},d_{\max}] \tag{11}$$

- where: d ranges from 1 μm (10^{-6} m) to 1 mm (10^{-3} m).

4) Turbulent mixing: Turbulent mixing plays a critical role in redistributing oil droplets vertically in the water column, driven by factors such as wind speed, current shear, stratification, and the dissipation of wave energy. The strength of this vertical mixing is quantified by the vertical eddy diffusivity coefficient, $K(z)$, as described by Visser [36]. In Lagrangian particle tracking models, the vertical movement of oil droplets is commonly simulated using a random walk approach. This stochastic method accounts for both deterministic and random influences on particle displacement. The vertical displacement of a droplet (Δz) over a time interval (Δt) can be calculated as:

$$\Delta z = K'\left(z_n\right)\Delta t + R\sqrt{\frac{2}{r_s}K\left(z_n + \frac{K'\left(z_n\right)\Delta t}{2}\right)\Delta t} \tag{12}$$

- where: $K'(z_n)$ is the derivative of the eddy diffusivity coefficient ($K(z)$) with respect to the vertical coordinate (z) at the position of the particle (z_n), R is a random number with a mean of zero ($\mu_{<R^2>} = 0$) and standard deviation of r ($\sigma_{<R^2>} = r_s$), the first term represents the non-random advective component, which moves the particle from regions of low diffusivity to regions of high diffusivity and the second term adds the random fluctuation based on the local diffusivity at a position slightly offset from the current particle location [36].

2.3. Oil Weathering Process

OpenOil integrates advanced parameterizations of key oil weathering processes, including 1) dispersion, 2) evaporation, 3) emulsification, and 4) biodegradation. These processes are modeled using oil properties sourced from NOAA's ADIOS (Automated Data Inquiry for Oil Spills) Oil Library. The evaporation rate varies considerably depending on oil type and environmental conditions such as wind speed [31]. Both evaporation and emulsification substantially alter the oil's density, viscosity, and interfacial tension, which in turn affect the droplet size distribution [23].

1) Dispersion: The dispersion process simulates the entrainment of oil droplets into the water column, primarily driven by turbulence generated at the ocean surface by wind and waves [37]. In OpenOil, dispersion is modeled using the Delvigne and Sweeney [35] approach, which estimates wave energy dissipation—the energy lost due to wave breaking—calculated as:

$$D_e = 0.0034 \times g\rho_{sw}H_s^2 \tag{13}$$

A critical parameter is the wave energy dissipation coefficient (c_{disp}), representing the fraction of dissipated energy contributing to oil dispersion:

$$c_{disp} = \left(D_e\right)^{0.57} f_{bw} \tag{14}$$

- where: f_{bw} (the fraction of breaking waves) is set to 0.02.

The oil dispersion rate into the water column (q_{disp}) is then computed as:

$$q_{disp} = \frac{c_{Roy} c_{disp} V_{entrain}}{\rho_{oil}} \tag{15}$$

- where: $c_{Roy} = 2400 \times exp\left(-73.682 \times \sqrt{\frac{\mu_{oil}}{\rho_{oil}}}\right)$ is Roy's constant, accounting for the oil's viscosity and density effects, and $V_{entrain} = 3.9 \times 10^{-8}$ m^3/s is the entrainment volume constant, representing the oil volume mixed into the water per second.

2) Evaporation: OpenOil adjusts its evaporation modeling based on the prevailing conditions of the oil slick [24]. Under calm weather, when the slick remains smooth and undisturbed, evaporation is simulated using Mackay's analytical model [38]. In contrast, during rough sea states, OpenOil applies a more detailed approach based on the ADIOS2 framework, which employs a pseudo-component evaporation model [39]. In this model, crude oils and refined products are represented by a limited set of discrete, non-interacting components, each characterized by its own vapor pressure. The evaporation rate of each component depends on factors including wind speed, sea surface temperature, slick thickness, the component's molar fraction, and its volume. The molar volume of each pseudo-component is estimated using empirical correlations with alkane boiling points, enabling the calculation of vapor pressure through Antoine's equation [40].

3) Emulsification: OpenOil simulates emulsification following the approach of Lehr *et al.* [24], incorporating key factors such as oil weathering, evaporation, water content, and droplet size distribution. Once emulsification initiates, the model calculates the growth of the oil–water interfacial area over time, driven by wave energy and wind speed. This interfacial area is capped by a maximum value (S_{max}) of 5.4×10^7 m^2, determined by the oil's properties and droplet characteristics. The water fraction (Y) within the emulsion is dynamically updated based on the relationship between interfacial area and droplet size, expressed as:

$$Y = \frac{Sd_w}{6 + Sd_w} \tag{16}$$

- where: S is the oil–water interfacial area and d_w is the average water droplet diameter.

4) Biodegradation: Biodegradation plays a critical role in the natural attenuation of marine oil spills, gradually reducing their environmental impact. The rate of biodegradation depends on factors such as hydrocarbon type, temperature, microbial communities, and the availability of oxygen and nutrients. In OpenOil, the biodegradation process follows the model proposed by Adcroft *et al.* [41], emphasizing the influence of temperature. The total biodegradation time (R^{-1}), expressed in days, is calculated as:

$$R^{-1} = 12 \text{ days} \times 3^{(20^\circ\text{C} - T)/10^\circ\text{C}} \tag{17}$$

- where: T is the water temperature. This equation estimates the time required for microbial colonization and the degradation of the most persistent oil components, accounting for both dissolved and undissolved oil fractions.

2.4. Simulation Setup and Study Area

The numerical simulation for oil spill dispersion was conducted using the OpenOil model, a Lagrangian particle-tracking system integrated with atmospheric and oceanographic forcing data. The case study examined a continuous oil spill caused by a shipwreck off the coast of Tobago on February 7, 2024 (**Figure 1**). The model incorporated multiple environmental datasets—including wind fields, ocean currents, bathymetry, and wave data—to simulate the trajectories of oil particles and their interaction with the marine environment. The spill involved an estimated 35,000 barrels of oil. Using a standard conversion factor (1 barrel = 0.1589872949 m^3) and the given oil density of 854.2 kg/m^3, this volume corresponds to approximately 5564.56 cubic meters (m^3) of oil. An overview of the input parameters and data sources is provided in **Table 1**.

To analyze the transport characteristics of simulated oil particles, we implemented a computational approach within the OpenOil python framework. This involved extracting movement data, calculating directional trends, and assessing key transport metrics such as distance and velocity. Longitude and latitude coordinates were retrieved at each time step, and their differences were used to compute displacement, movement angles, and the dominant movement direction. Trajectory characteristics, including total distance traveled, segment-wise distances, and particle velocities, were derived and stored for further analysis. Mean speed and travel distance were also calculated, excluding stationary particles to ensure accuracy. The initial release point of the Tobago shipwreck oil spill was derived from the Trinidad and Tobago Weather Center [13].

Table 1. Simulation configurations: Parameters and settings used in the oil spill model.

Study Area	Tobago island, Caribbean
Date start (UTC)	7 February 14:00
Geographical Coordinates	60.7827˚ W, 11.13389˚ N
Oil Type	Generic Light Crude
Discharge Rate	31.62 m^3/h
Particle Release	200 particles/h
Total Seeding Elements	35200
Seeding Radius	15 meters
Oil Spill Duration	176 hours (continuous spill)
Droplet Size Distribution	1 μm - 1 mm
Wind Drift Factors	0% - 6%
Processes Considered	Evaporation, emulsification, dispersion, biodegradation, wind drift, vertical mixing, wave entrainment, coastline stranding
Simulation Duration	176 hours (hourly outputs) in a NetCDF file

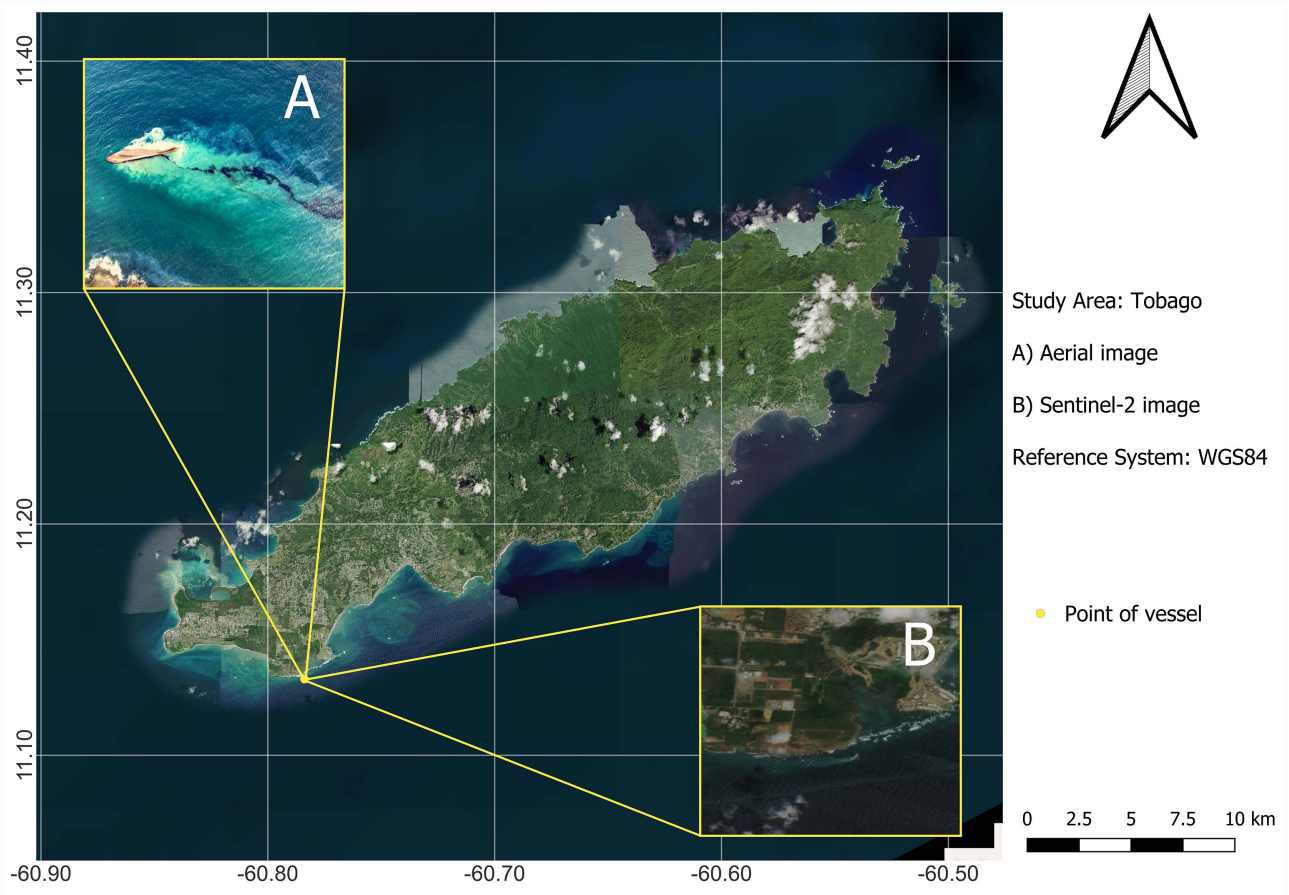

Figure 1. Geographic visualization of areas of interest related to the Tobago shipwreck. The red marker indicates the initial release point of the shipwreck. (A) shows an aerial view of the region, while (B) presents a Sentinle-2 satellite image of the same area, providing a more detailed perspective.

2.5. Satellite Image Acquisition and Preprocessing

To validate the simulated oil spill trajectories, high-resolution satellite imagery was obtained from the Copernicus Data Space Ecosystem. Both optical and radar datasets were selected to coincide with critical dates in the spill's progression.

- For 12 February 2024, a Level-2A Sentinel-2 scene was used, containing the visible RGB bands (B2, B3, B4) at a spatial resolution of 10 meters. As the product is atmospherically corrected via the Sen2Cor processor, it provides surface reflectance values suitable for detecting oil slicks under favorable viewing conditions. The selected image offered clear visibility of the sea surface, enabling effective visual assessment of oil-affected areas.
- For 14 February 2024, Sentinel-1 synthetic aperture radar (SAR) data was retrieved in Ground Range Detected (GRD) format. The acquisition was performed in Interferometric Wide (IW) swath mode. The IW mode collects data in dual-polarization (VV and VH), but only the VV polarization was used due to its higher signal-to-noise ratio. The GRD product undergoes radiometric calibration and thermal noise removal.

In both cases, photointerpretation techniques were employed to manually de-

lineate the extent of the surface oil slicks. The affected areas were digitized based on variations in tone, texture, and spatial context, informed by knowledge of local wind and current conditions. The delineated areas were exported as vector shapefiles and reprojected to a common coordinate system (WGS84). The resulting masks served as ground truth for quantitative comparison with OpenOil simulation outputs.

2.6. OpenOil's Performance Metrics

To assess the performance of the OpenOil model, the forecasted oil slick coverage was compared with the actual oil slick extent observed through in situ observations, Sentinel-1 and Sentinel-2 images. The comparison led to the establishment of two key performance metrics. While the first have been widely used in flood modeling for comparing model results with satellite data [42], the second metric has recently been introduced to oil spill modeling [43] [44].

1) Success Rate (*SR*): The *SR* measures the overlap between the model's predicted oil spill area and the actual spill area as derived from observations and satellite images. It is calculated as:

$$SR = \frac{Overlapped\ area}{Total\ actual\ area} \tag{18}$$

- where: the *Overlapped area* refers to the intersection between the image-derived oil slick and the modeled spill, while the *Total actual area* represents the oil spill area as observed in the images. The *SR* ranges from 0 (indicating no overlap) to 1 (indicating perfect overlap). It is important to note that SR does not account for any modeled oil spill area outside the actual spill extent.

2) Centroid Skill Score (*CSS*): The Centroid Skill Score (*CSS*) evaluates how closely the predicted centroid of the oil spill matches the observed centroid. It begins by calculating the Initial Centroid Displacement Index (*CI*), which measures the distance between the centroids of the actual and modeled oil spill areas. The *CI* is defined as:

$$CI = \frac{\Delta x_{centroid}}{L_{box}} \tag{19}$$

- where: $\Delta x_{centroid}$ is the distance between the geometric centers (centroids) of the actual and modeled oil spill areas at a given time and L_{box} is the length of the diagonal of the bounding box that encloses the observed oil spill area.

The Centroid Skill Score (*CSS*) is then calculated as:

$$CSS = \begin{cases} 1 - \dfrac{CI}{C_{thr}} & \text{if } CI < C_{thr} \\ 0 & \text{if } CI \geq C_{thr} \end{cases} \tag{20}$$

- where: C_{thr} is a threshold distance, chosen by the user, that determines the tolerance for centroid displacement. In this study, $C_{thr} = 1$, meaning the model is considered valid if the distance between the observed and predicted centroids does not exceed the magnitude of the observed length scale.

3. Results

The simulation tracked the transport and weathering of a continuous spilled oil from February 7 to 14, 2024, under the combined influence of ocean currents, wind, and environmental conditions. Oil particles dispersed, submerged, stranded, or remained on the surface as they moved, while physical and chemical weathering processes altered their properties over time. Droplet size distributions, emulsion viscosity, and water content were also monitored throughout the simulation. The analysis focuses on three key dates - February 9, 12, and 14, 2024 - to evaluate the evolution of oil distribution, supported by quantitative metrics and statistics.

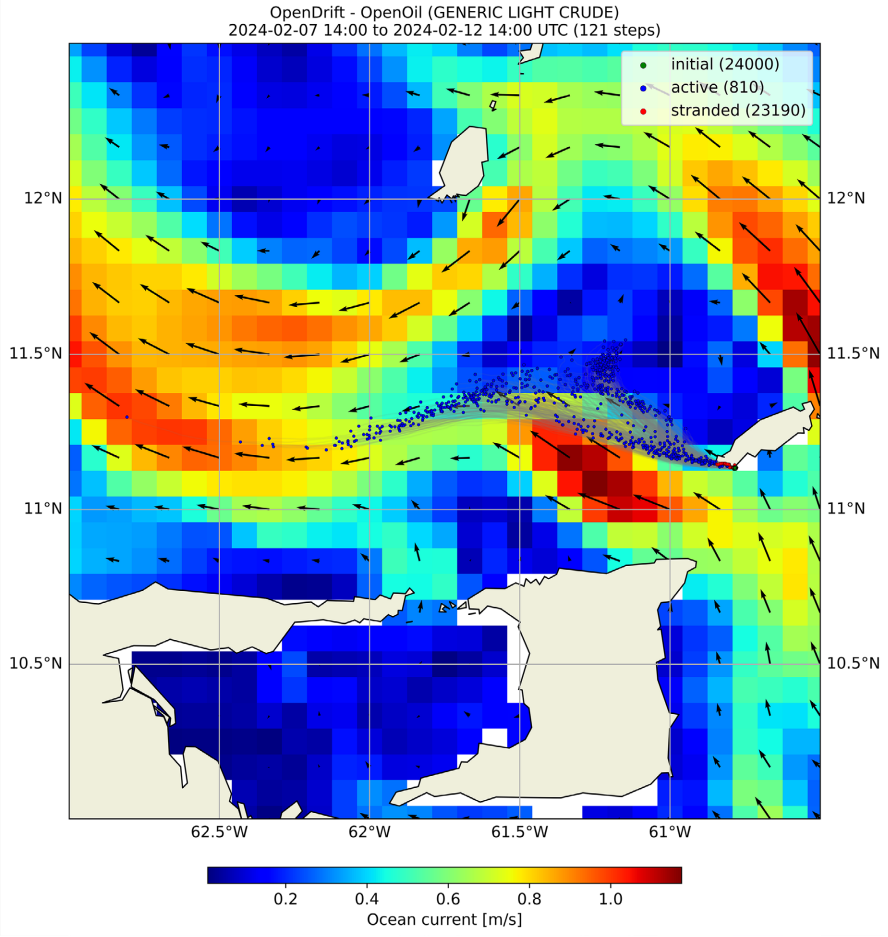

Figure 2. (a) Sentinel-2 satellite image of the Baniyas oil spill on June 25, 2019. The red overlay indicates the extent of the oil spill, identified using photo-interpretation techniques. (b) Wind speed distribution over the Baniyas open sea region on the same day. Colored points represent oil particles.

Figure 2 illustrates the dispersion of oil particles (Generic Light Crude) over a simulation period from February 7 to February 12, 2024, in relation to ocean currents. The background is a color map representing ocean current speeds, ranging from blue (low velocity, ~0.0 m/s) to red (high velocity, ~1.0 m/s). Superimposed

black arrows indicate the direction and relative magnitude of surface currents across the study area. At the start of the simulation, the initial oil release (24,000 particles, marked in green) occurs offshore, where currents are moderate to strong, flowing predominantly from east to west-southwest across the central portion of the map. The prevailing surface currents, with speeds ranging from ~0.1 m/s to over 0.8 m/s, drive the oil westward and southwestward toward the coastline. As the spill progresses, the interaction between stronger western currents (orange-red regions) and weaker northern eddies (blue-green areas) creates a divergence in particle pathways. A significant portion of the oil becomes stranded along the coast (23,190 particles, marked in red), indicating that coastal currents and topography play a crucial role in trapping oil close to shore. Meanwhile, a smaller number of active particles (810, marked in blue) continue to circulate offshore, primarily following the southern boundary current toward the southwest. Localized eddies north of the spill site appear to slow the dispersion in that area, temporarily trapping some particles in circular flow patterns before they are either carried toward shore or southward by stronger jets. These mesoscale features increase the complexity of the spill trajectory, leading to patches of higher oil concentration. Wind effects are not explicitly shown but would likely enhance the southwestward drift, complementing the ocean current patterns. The predominance of stranding suggests that both currents and potential wind-induced drift are effectively funneling the oil toward the southeastern coastline, leading to high shoreline impact. Overall, the spill evolution demonstrates a constrained dispersal dominated by southwestward advection, coastal trapping, and limited offshore spreading, with nearly all particles either stranded or nearshore by the end of the simulation period.

Figure 3 illustrates the simulated trajectories of oil particles influenced by wind drift over a 121-step period (February 7 to February 12, 2024), modeled using OpenDrift-OpenOil for generic light crude. The color gradient represents the wind drift factor, ranging from low (blue) to high (red), showing the varying degrees of wind influence on particle movement. At the onset of the simulation, oil particles (24,000 initial, marked in green) disperse outward from the release point, primarily following the prevailing westward and southwestward ocean currents. As the simulation progresses, the influence of wind drift becomes more apparent, with trajectories shifting and elongating away from the main current pathway. Particles exposed to higher wind drift factors (orange to red trajectories) display a stronger deviation toward the southwest and southeast, extending farther offshore and accelerating their movement away from the source. This drift-driven spread creates a broader dispersal fan compared to the lower wind drift pathways (blue and green), where particles remain more clustered and localized along the coastal margin. The asymmetry in the trajectory spread reflects the cumulative interaction between wind and current forces: while currents steer particles westward, stronger wind drift pulls particles further south and southeast, increasing the distance from the spill origin. Over time, these combined forces result in a

wider and more dispersed contamination pattern, with stranded particles (23,190, marked in red) accumulating along the southeastern coastline, and a smaller number (810, marked in blue) remaining active offshore.

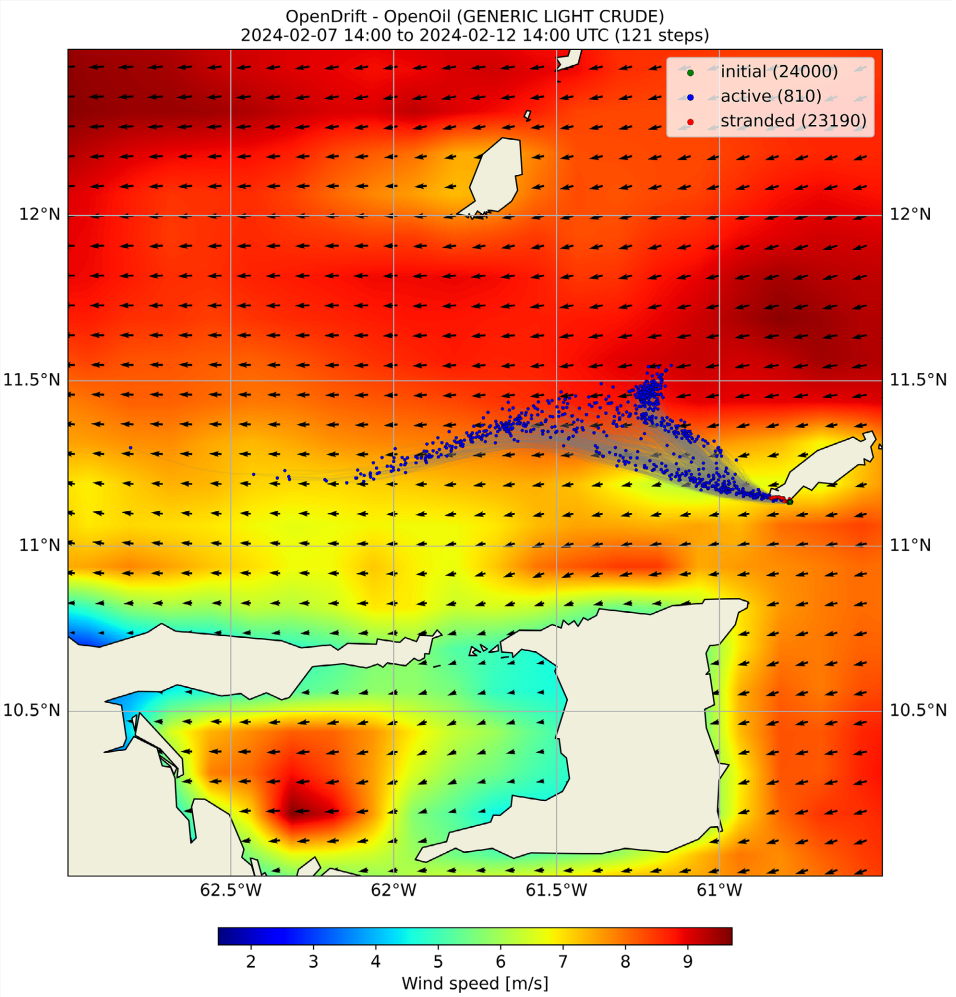

Figure 3. Simulated trajectories of oil particles influenced by wind drift over a 5-day period, as computed by the OpenOil model. The color gradient represents the wind drift factor, from low (blue) to high (red). Green dots indicate initial oil particle positions, blue dots show their active positions at the end of the simulation, and red dots represent stranded oil particles along the shoreline.

Figure 4 presents the oil droplet size distribution simulated by the OpenOil model. The left panel (**Figure 4(a)**) shows the volume spectrum, where droplet volume is distributed across a wide range of diameters. The histogram does not display a strong skew toward smaller or larger droplets; instead, it indicates a relatively broad and variable spread of oil volume contributions across droplet sizes. The right panel (**Figure 4(b)**) presents the cumulative volume spectrum, which increases nearly linearly with droplet diameter. This trend suggests that the total oil volume is more evenly distributed across droplet sizes, with no single size range dominating the overall dispersed oil volume.

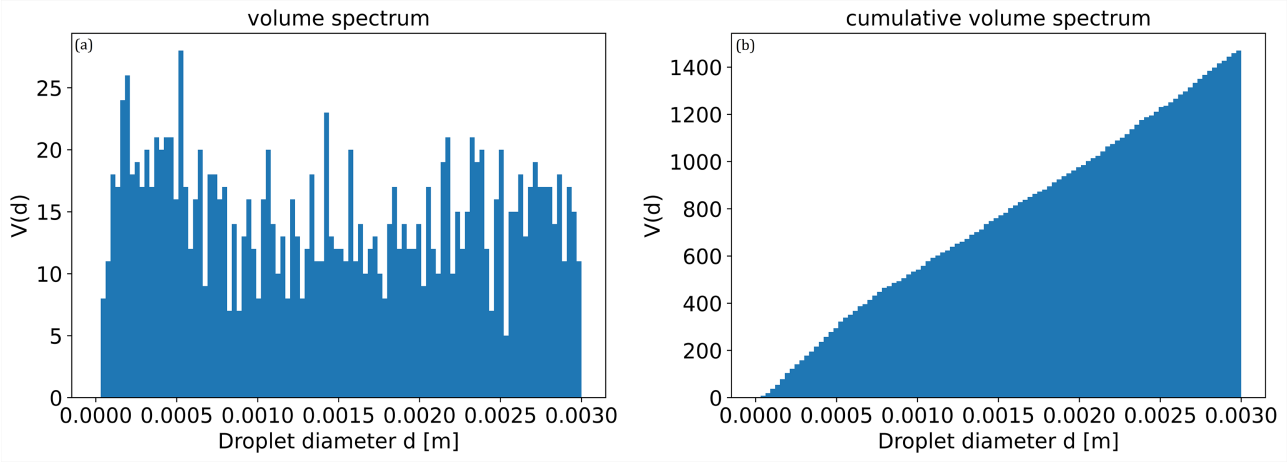

Figure 4. Droplet size distribution analysis of oil droplets simulated by OpenOil: (a) volume spectrum of oil droplets; (b) cumulative volume spectrum.

Figure 5(a) presents the evolution of the oil budget over a simulation period of 176 hours for a spill of generic light crude oil (854.2 kg/m^3), capturing the complex interactions of physical and chemical processes affecting the oil's fate in the marine environment. Beginning with an initial release of oil, the mass distribution among different compartments - dispersed, submerged, surface-bound, stranded, evaporated, and biodegraded - changes progressively over time. Notably, the oil remains predominantly stranded throughout the simulation, accumulating rapidly in the early hours and continuing steadily up to 4.5 million kg by the end of the 176-hour period, indicating significant shoreline interaction or sedimentation. The submerged fraction rises gradually in the initial phase but plateaus at a relatively low mass compared to the stranded fraction, suggesting limited entrainment below the surface layer. Both the dispersed and evaporated fractions remain minor components over the entire duration, with minimal increases after the first 50 hours. The biodegraded fraction increases slowly, indicating that biological degradation processes are just beginning to take effect within the simulation timeframe, remaining significantly lower than other pathways.

In the middle panel (**Figure 5(b)**), the evolution of oil properties is depicted through the progression of emulsion viscosity (green shaded area) and water content (blue line). Emulsion viscosity begins to increase markedly after 80 hours, reaching values above 80,000 mPa·s by the end of the simulation. This sharp increase in viscosity reflects the oil's transition into a highly stable water-in-oil emulsion, significantly thickening over time. Meanwhile, the water content increases rapidly from 50 hours onward, eventually exceeding 70% by 160 hours, showing continuous water incorporation into the oil matrix. The widening shaded area indicates growing variability in these properties, likely due to spatial heterogeneity or progressive emulsification across different oil patches.

The bottom panel (**Figure 5(c)**) presents the wind speed (blue line) and current speed (red line) over the same period. Wind speed remains relatively stable, fluctuating slightly around 7 m/s, suggesting moderate meteorological forcing that

may promote limited mixing and emulsification. In contrast, the current speed increases gradually from 0.35 m/s to just above 0.4 m/s by the end of the simulation. This steady rise in current speed implies a slow intensification of horizontal transport, though not sufficient to cause dramatic redistribution of oil masses in the absence of stronger winds or turbulent conditions. Overall, the figure indicates that under the simulated conditions, the majority of the oil becomes stranded relatively quickly, with limited dispersion or evaporation, while water uptake and viscosity increase progressively, promoting the formation of a viscous, stable emulsion with reduced mobility and degradation over time.

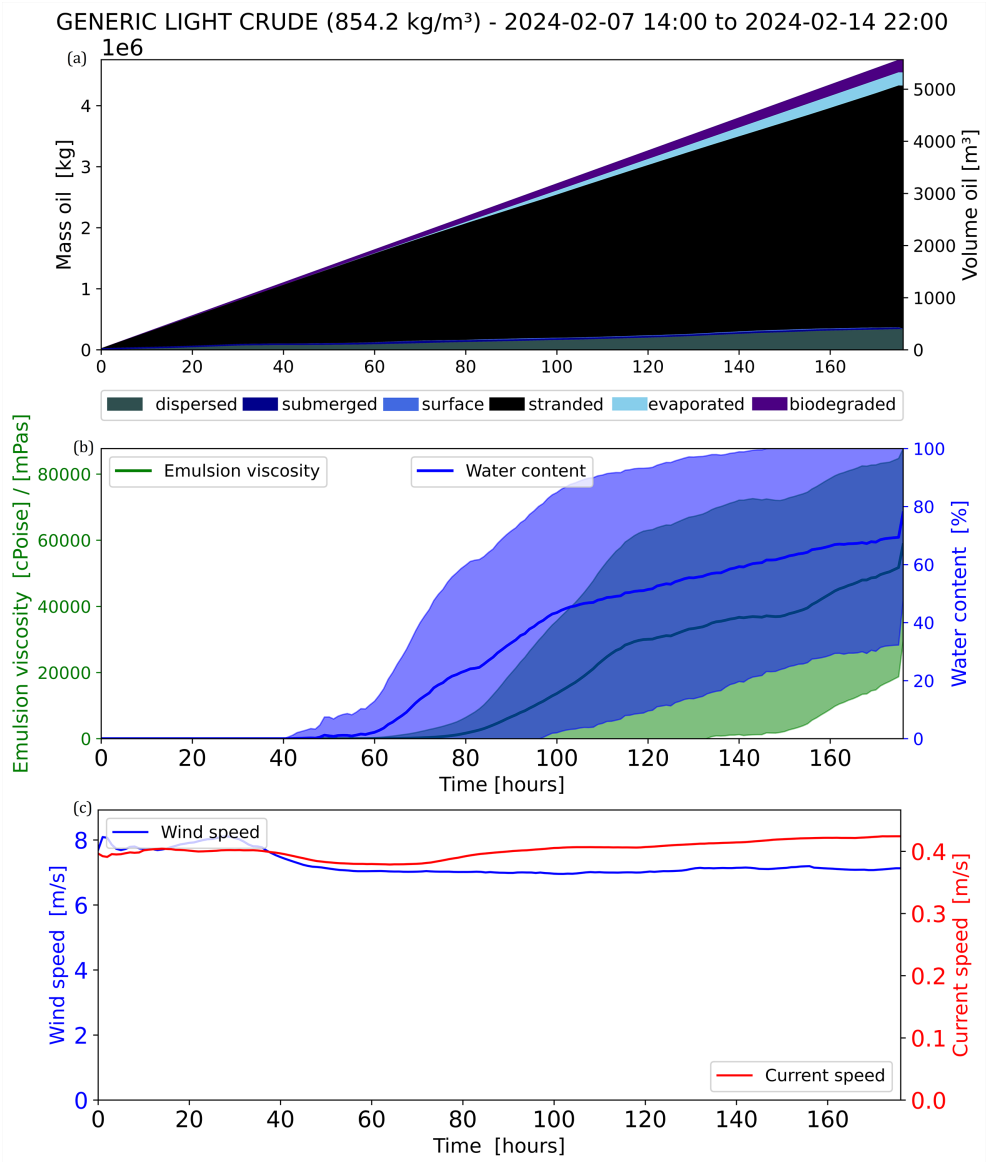

Figure 5. Evolution of the oil budget and environmental conditions over time for a simulated release of generic light crude oil. (a) Time evolution of oil mass distribution among dispersed, submerged, surface, stranded, evaporated, and biodegraded compartments; (b) evolution of emulsion viscosity (green) and water content (blue); (c) wind speed (blue) and current speed (red) over the simulation period of 176 hours.

1st key date - 9 February 2024: To evaluate the accuracy of the oil spill prediction, OpenOil simulation outputs were compared to in-situ measurements collected on 9 February 2025 at 19:00 UTC (**Figure 6**). To ensure consistency with satellite-visible oil extents, only particles in the OpenOil simulation with depths between 0 and 0.1 m were included in the visualization. Deeper particles were excluded from the analysis, as they do not contribute to the surface signature observed in either satellite imagery or field measurements [45]. The simulation model predicted the spread of the oil plume toward the southeast of the initial release point, with higher concentrations located nearshore and along the southwestern coast. The in-situ measurements [13], visualized in green, show good spatial overlap with the model's predicted oil trajectory, particularly in the central and western sections of the plume. However, some discrepancies were observed at the plume's eastern extent, where the model slightly overestimated the spread. Based on [13], the observed oil slick extended approximately 1400 m in length and 560 m in width at its widest point.

Quantitative metrics support the visual and statistical assessments:

- SR = 0.80, indicating 80% spatial agreement between the model and measurements.
- CI = 0.103, reflecting a relatively narrow dispersion in spatial error.
- CSS = 0.89, suggesting strong overall agreement between modeled and observed data.

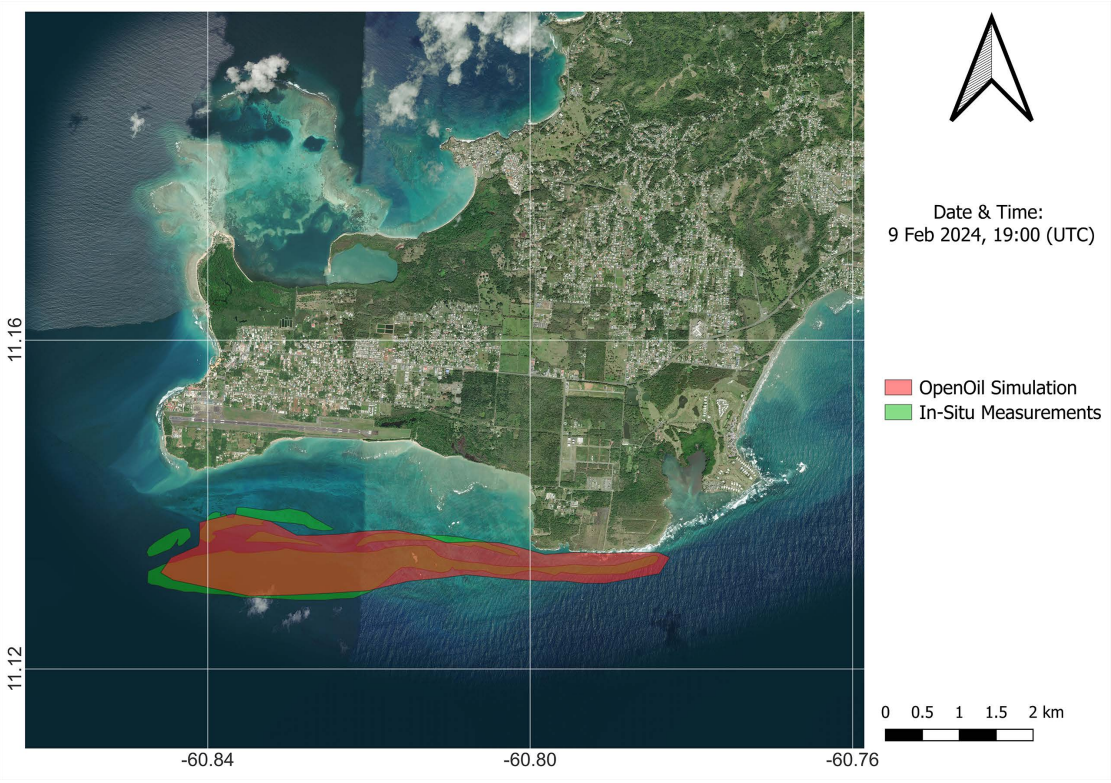

Figure 6. Geospatial comparison of oil spill extent from OpenOil simulation and in-situ measurements on 9 February 2024 at 19:00 UTC.

The histogram of total distances corresponding points in the OpenOil datasets (Figure 7) provides a statistical view of the spatial agreement. The distribution is right-skewed, with the majority of distances falling below 1200 meters. The mean spatial deviation was 736.39 m, while the median was 770.86 m. These values suggest that the central tendency of the model prediction is relatively close to the observed field data, though a long tail in the histogram indicates occasional outliers.

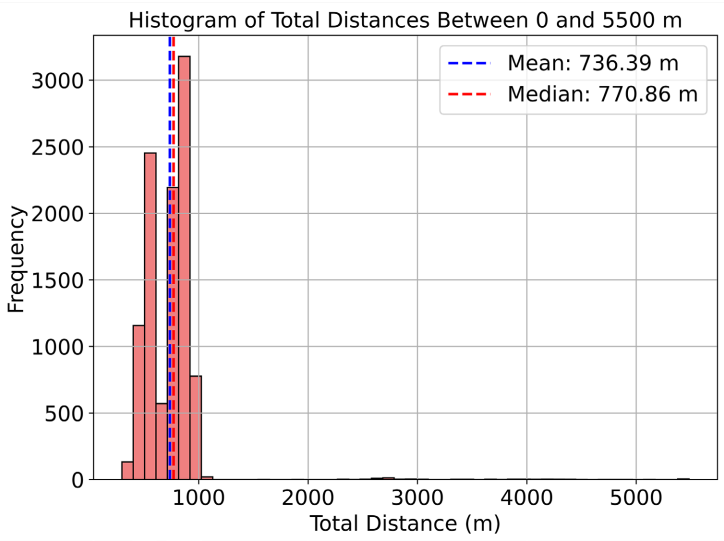

Figure 7. Histogram of spatial distances from OpenOil simulation predictions for 9 February 2024.

2nd key date – 12 February 2024: To evaluate model accuracy on 12 February 2024 at 14:00 UTC, the predicted oil distribution from the OpenOil simulation was compared with Sentinel-2 satellite imagery (Figure 8). As with the previous analysis, only surface particles within the 0 - 0.1 m depth range were included to reflect oil observable from space, while deeper submerged particles were excluded. The OpenOil simulation indicates a wide westward dispersion of the oil slick, extending over approximately 40 kilometers from the initial spill location. The general direction and shape of the predicted plume show strong agreement with the satellite-observed extent, particularly along the central axis and western margin. However, some mismatches can be observed at the northern edges, where simulated concentrations appear more extensive than those visible in the satellite data.

Despite these localized differences, quantitative comparison demonstrates strong performance of the simulation:

- SR = 0.71, indicating that 71% of the predicted spill overlapped with the satellite-observed area.
- CI = 0.0151, reflecting minimal spread in spatial discrepancies, which supports the visual consistency.
- CSS = 0.98, indicating a very high overall agreement between simulated and observed oil extents.

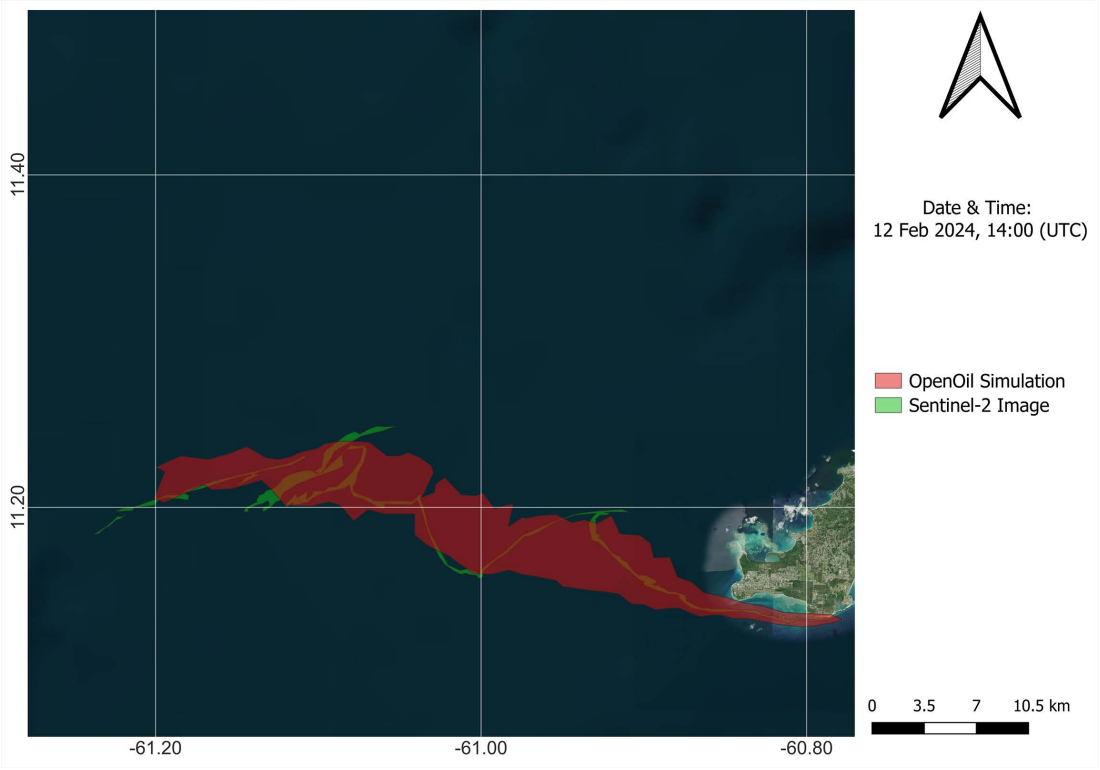

Figure 8. Geospatial comparison of oil spill extent from OpenOil simulation and Sentinel-2 satellite image on 12 February 2024 at 14:00 UTC.

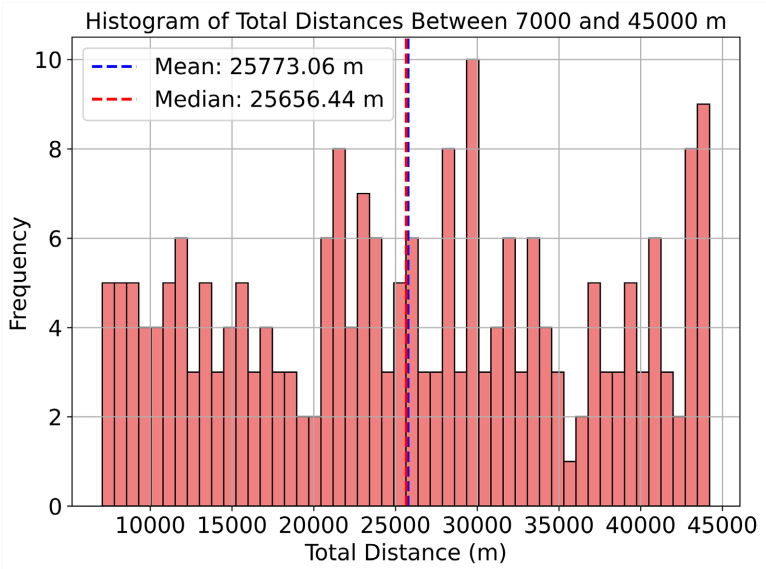

Figure 9. Histogram of spatial distances from OpenOil simulation predictions for 12 February 2024.

This strong CSS value suggests that, despite a slightly lower overlap ratio (SR), the simulation captured the overall spatial trend of the oil slick with high fidelity and minimal error dispersion. The results for this date highlight the model's ability to reproduce long-range drift patterns accurately under prevailing oceano-

graphic and atmospheric conditions.

The accompanying distance histogram (Figure 9) offers a statistical perspective. Distances between paired simulated and observed points range from 7 km to 45 km, with the distribution centered near 26 km. The mean deviation is 25,773 m, and the median is 25,656 m, indicating a nearly symmetric spread about the central tendency. While the tail toward the upper end reveals a subset of mismatched points - primarily at the plume extremities - the bulk of the distances cluster tightly around the mean, supporting the high CSS value.

3rd key date – 14 February 2024: Model skill was further assessed by confronting the OpenOil forecast with a Sentinel-1 SAR slick outline acquired at 22:00 UTC (Figure 10). Again, only particles occupying the upper 0 - 0.1 m were retained to match the radar-detectable surface film. The forecast transported the plume west-north-west from the release site, stretching more than 45 km offshore and developing several filamentous "fingers" at its leading edge. The Sentinel-1 extent (green) overlaps the simulated core along most of the central reach, yet two systematic differences emerge: i) the model overshoots the slick length, producing a longer western tail with three narrow filaments not captured by the satellite, and ii) near the headland the simulation depicts a broader fan that wraps south of the observed outline. These mismatches suggest that wind-driven shear and submesoscale eddies - poorly resolved in the forcing - became increasingly important after four days of drift.

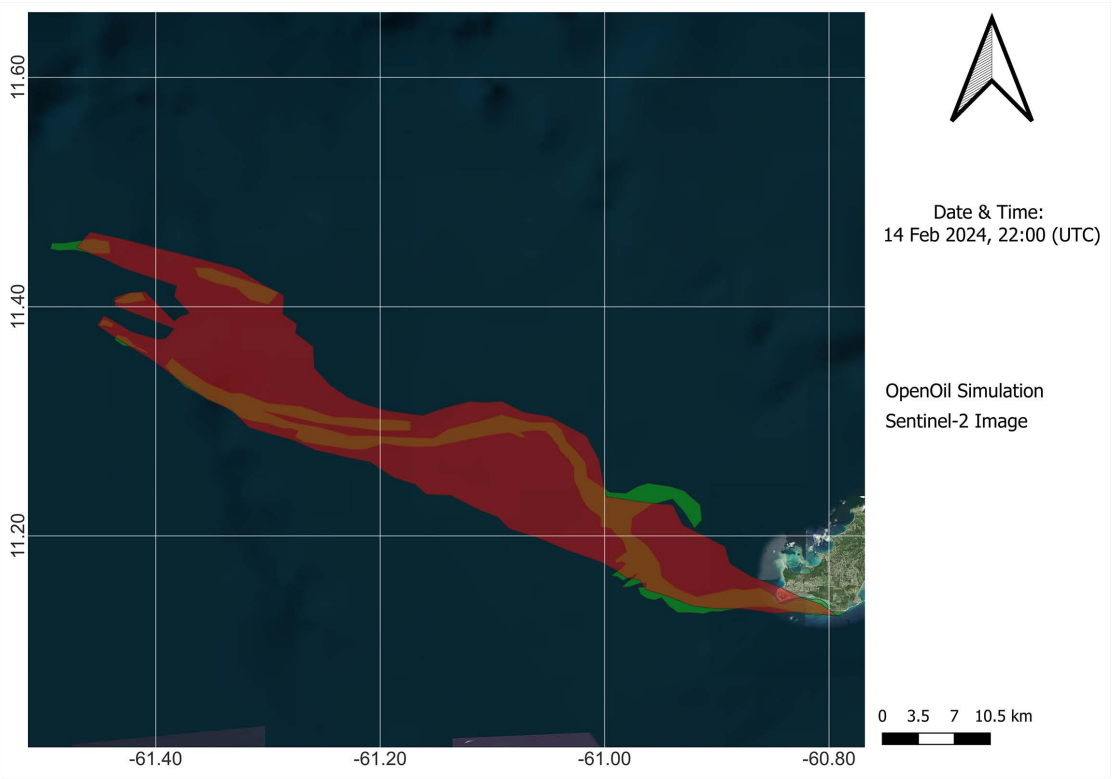

Figure 10. Geospatial comparison of oil spill extent from OpenOil simulation and Sentinel-1 SAR observations on 14 February 2024 at 22:00 UTC.

Quantitative metrics echo the visual appraisal:

- SR = 0.85, roughly 85 % of the simulated footprint coincides with the Sentinel-1 slick, denoting good spatial overlap despite the elongated forecast tail.
- CI = 0.074, a wider confidence interval than earlier dates, consistent with the greater dispersion of distance errors introduced by the over-extension.
- CSS = 0.92, a high composite score, confirming that the core of the plume is still reproduced accurately once both spatial coverage and concentration are considered.

The distance histogram (Figure 11) reinforces these findings. Paired point separations span 45 - 85 km, with multiple peaks around 55 km, 65 km, and 80 km, reflecting the filament structure in the western plume. The mean deviation is 69,445 m, and the median is 70,774 m, signifying a fairly symmetrical but broadly spread distribution. While the long-distance modes correspond to the model's over-extended filaments, the dominant central mode aligns with the high-overlap core, explaining the still-robust CSS score.

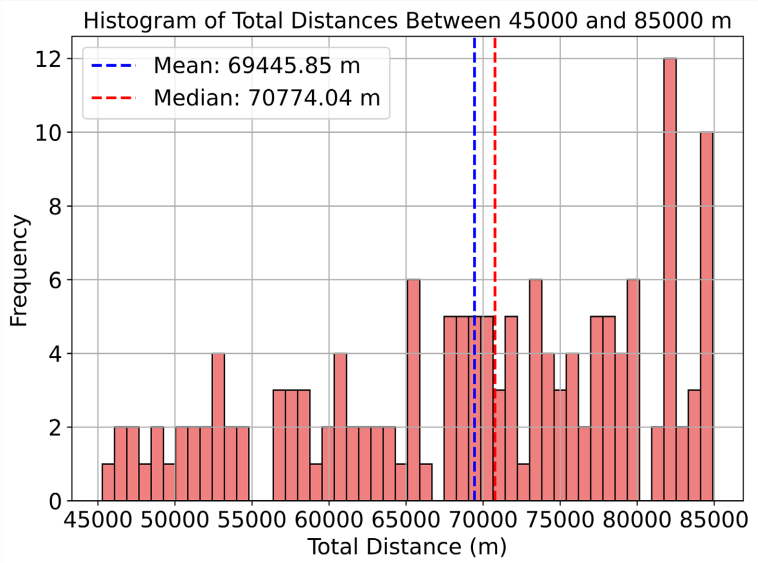

Figure 11. Histogram of spatial distances from OpenOil simulation predictions for 14 February 2024.

4. Discussion and Limitations

OpenOil incorporates detailed parameterizations of physical and chemical processes affecting oil transport. Despite this, the simulation results are highly sensitive to several input assumptions and model parameters. In particular, the initial oil droplet size distribution plays a critical role in governing vertical movement and residence time, which in turn affects dispersion patterns. The wind drift factor, varying between 0% and 6%, also significantly influences both the extent and direction of oil transport, as demonstrated in Table 2, where mean distances increase non-linearly with higher wind drift values. Additionally, the accuracy of ocean current fields is pivotal in determining coastal stranding patterns. Although

these sensitivities are evident, a formal sensitivity analysis was not conducted in this study. Uncertainty quantification was limited to indirect assessments using validation metrics such as the Correlation Skill Score (CSS) and Success Rate, leaving the effect of small perturbations in input parameters on model outputs largely unknown. Future studies should employ ensemble-based approaches or Monte Carlo simulations to better quantify uncertainty ranges and improve forecast robustness, particularly in operational spill response scenarios. Table 2 summarizes the simulation configurations used to evaluate wind drift effects on oil transport:

Table 2. Simulation configurations showing the effect of wind drift factor on oil spill transport.

Wind drift factor	Wind Speed (m/s)	Mean Distance (m)
1%	0.1928	844.66
2%	0.2063	954.30
3%	0.2316	1131.83
4%	0.3475	2356.23
5%	0.5237	5437.82
6%	0.6077	8044.75

While this study demonstrates the effectiveness of the OpenOil module in simulating the transport and fate of oil from a shipwreck-origin continuous spill, several limitations must be acknowledged. First, the model's performance is highly sensitive to the spatial and temporal resolution of input datasets, particularly wind, wave, and current fields. Despite efforts to refine spatial resolution through interpolation, such enhancements yielded limited improvements in accuracy and significantly increased computational demand. Second, the model showed a tendency to overestimate the extent of the oil slick in certain regions, especially at later stages of the simulation, which may be attributed to the coarse resolution or limited temporal fidelity of environmental forcing data, as well as the absence of sub-mesoscale processes like wind shear, tidal jets, and eddy-resolving currents; future OpenOil runs could incorporate these processes using higher-resolution hydrodynamic models or nested grids to better capture local currents and shear effects, improving representation of fine-scale transport and reducing overestimation of oil spread. Third, although OpenOil incorporates a range of physical and chemical weathering processes, the timescales for evaporation and biodegradation were relatively short in this simulation, limiting the model's ability to fully capture long-term degradation dynamics. Furthermore, the lack of explicit uncertainty quantification or formal sensitivity analysis means that confidence bounds on model outputs could not be estimated—this limits the robustness of forecasts for decision support in operational contexts. Finally, while the model was calibrated using satellite and in-situ observations, its reliance on scenario-specific parameters and assumptions (e.g., droplet size distribution, oil type, release rate) may constrain its generalizability to other spill scenarios without additional tuning.

These limitations underscore the need for continued model refinement, especially regarding fine-scale ocean dynamics, uncertainty characterization, and automated data assimilation for future applications in spill response and environmental risk assessment.

5. Conclusions

The Tobago oil spill of February 2024, caused by the wreck of a vessel carrying crude oil near the southern coast of Tobago, provided a complex and high-impact case study for evaluating oil spill modeling tools in a dynamic and ecologically sensitive marine environment. The event's unique characteristics—including a continuous shipwreck-origin spill, delayed detection, and challenging oceanographic conditions—offered a rare opportunity to assess the performance of the OpenOil model in simulating the transport, dispersion, and weathering of oil in the southern Caribbean.

The OpenOil simulations, driven by regional current and wind data, demonstrated a high degree of fidelity in predicting oil transport and stranding patterns. Across three key evaluation dates (February 9, 12, and 14), the model captured the observed spread of the oil slick with substantial accuracy, as validated against in-situ measurements and high-resolution satellite data from Sentinel-2 and Sentinel-1. Quantitative metrics—including spatial overlap ratios (SR), confidence intervals (CI), and composite similarity scores (CSS)—consistently indicated strong model performance, with CSS values ranging from 0.89 to 0.98. Despite some discrepancies, particularly in simulating filamentous features and slight overestimations at the plume's edges, the model successfully represented the core spatial dynamics and directional trends of the spill.

Crucially, the study also highlighted OpenOil's capability to simulate critical physical and chemical processes affecting oil fate. The evolution of droplet size distributions, emulsion viscosity, and water content reflected realistic behavior, closely aligning with empirical observations and theoretical expectations. The model's droplet dynamics showed strong agreement with published data, underscoring its reliability for predicting vertical transport and residence times of dispersed oil. Furthermore, oil mass budget analysis revealed a rapid accumulation of stranded oil, limited evaporation and biodegradation, and significant emulsion formation—key factors contributing to the spill's persistence and environmental threat.

Overall, this study confirms OpenOil's utility as a robust and validated tool for forecasting oil transport and weathering in complex marine systems, particularly in regions with limited real-time observational infrastructure. However, it also underscores the importance of high-resolution forcing data and the need to improve model representation of sub-mesoscale processes such as wind shear and eddy interactions. Continued integration of satellite imagery, *in-situ* data, and advanced modeling will be vital for enhancing spill response strategies and minimizing ecological and economic damage in future incidents.

Acknowledgements

Part of this research has been carried out within the Horizon Europe Research and Innovation Programmes PERIVALLON and WATERVERSE.

Author Contributions

V.P. conceived the study and wrote the abstract; **V.P.** and **C.A.** wrote introduction, methodology and results; **A.M.** reviewed the first draft; **A.M.** and **I.G.** supervised the methodology and conclusions sections; **S.V**. and **I.K.** funding acquisition. All authors have read and agreed to the published version of the manuscript.

Data Availability Statement

Available upon request.

Funding

This research was funded by the Horizon Europe Research and Innovation Programme through the PERIVALLON project (Grant Agreement No. 101073952) and the WATERVERSE project (Grant Agreement No. 101070262). The article reflects only the authors' views, and the commission is not responsible for any use that may be made of the information it contains.

Conflicts of Interest

The authors declare no conflict of interest.

References

[1] Yang, J., Hu, Y., Zhang, J., Ma, Y., Li, Z. and Jiang, Z. (2023) Identification of Marine Oil Spill Pollution Using Hyperspectral Combined with Thermal Infrared Remote Sensing. *Frontiers in Marine Science*, **10**, Article 1135356. https://doi.org/10.3389/fmars.2023.1135356

[2] National Oceanic and Atmospheric Administration (2024) Oil Spills: Environmental Impacts and Response. https://www.noaa.gov/education/resource-collections/ocean-coasts/oil-spills

[3] ScienceDaily (2024) Deepwater Horizon Oil Spill Study Could Lead to Overhaul of Cleanup Processes Worldwide. https://www.sciencedaily.com/releases/2024/01/240122144353.htm

[4] National Research Council (2024) Biological Effects of Oil Releases in Marine Environments. NCBI Bookshelf. https://www.ncbi.nlm.nih.gov/books/NBK220710/

[5] International Tanker Owners Pollution Federation (2024) Oil Tanker Spill Statistics 2024. https://www.itopf.org/knowledge-resources/data-statistics/oil-tanker-spill-statistics-2024/

[6] National Oceanic and Atmospheric Administration (2023) Fiscal Year 2023: Providing Scientific Expertise for Oil and Chemical Spill Response. https://response.restoration.noaa.gov/oil-and-chemical-spills/fiscal-year-2023-providing-scientific-expertise-oil-and-chemical-spill

[7] Psarros, G., Skjong, R. and Vanem, E. (2011) Risk Acceptance Criterion for Tanker Oil Spill Risk Reduction Measures. *Marine Pollution Bulletin*, **62**, 116-127. https://doi.org/10.1016/j.marpolbul.2010.09.003

[8] Abou Samra, R.M. and Ali, R.R. (2024) Tracking the Behavior of an Accidental Oil Spill and Its Impacts on the Marine Environment in the Eastern Mediterranean. *Marine Pollution Bulletin*, **198**, Article ID: 115887. https://doi.org/10.1016/j.marpolbul.2023.115887

[9] Kristiansen, S. and Haugen, S. (2022). Maritime Transportation: Safety Management and Risk Analysis. 2nd Edition, Routledge. https://doi.org/10.4324/9781003055464

[10] Dagestad, K., Röhrs, J., Breivik, Ø. and Ådlandsvik, B. (2018) OpenDrift V1.0: A Generic Framework for Trajectory Modelling. *Geoscientific Model Development*, **11**, 1405-1420. https://doi.org/10.5194/gmd-11-1405-2018

[11] Papaioannou, V. (2025) Assessment of Oil Spill Dispersion and Weathering Processes in Saronic Gulf. *Advances in Hydrology & Meteorology*, **2**, No. 5. https://doi.org/10.33552/ahm.2025.02.000550

[12] Barker, C.H., Kourafalou, V.H., Beegle-Krause, C., Boufadel, M., Bourassa, M.A., Buschang, S.G., *et al.* (2020) Progress in Operational Modeling in Support of Oil Spill Response. *Journal of Marine Science and Engineering*, **8**, Article 668. https://doi.org/10.3390/jmse8090668

[13] Trinidad and Tobago Weather Center (2024) Tobago Oil Spill: What You Need to Know. https://ttweathercenter.com/2024/02/11/tobago-oil-spill-what-you-need-to-know/

[14] European Space Agency (ESA) (2024) Tobago Oil Spill [Satellite Image]. https://www.esa.int/ESA_Multimedia/Images/2024/02/Tobago_oil_spill

[15] Ganase, A., Kanhai, A., Lochan, H. and Gooding, N. (2023) A Guide to Coral Reef and Seagrass Restoration in Tobago (Version 1). Marine Resilience Initiative, Institute of Marine Affairs. https://www.ima.gov.tt/wp-content/uploads/2023/09/IMA_RestorationGuide_Tobago-MARIN.pdf

[16] Tavares, R., Carreon-Zapiain, M.T. and Perez-Jimenez, J.C. (2024) Vulnerability of Elasmobranchs Caught by Artisanal Fishery in the Southeastern Caribbean. *Regional Studies in Marine Science*, **79**, Article ID: 103851. https://doi.org/10.1016/j.rsma.2024.103851

[17] Purohit, B.K., Tewari, S., Prasad, K.S.N.V., Talari, V.K., Pandey, N., Choudhury, P. and Panda, S.S. (2024) Marine Oil Spill Clean-Up: A Review on Technologies with Recent Trends and Challenges. *Regional Studies in Marine Science*, **80**, Article ID: 103876. https://doi.org/10.1016/j.rsma.2024.103876

[18] Dookie, I., Rocke, S., Singh, A. and Ramlal, C.J. (2018) Evaluating Wind Speed Probability Distribution Models with a Novel Goodness of Fit Metric: A Trinidad and Tobago Case Study. *International Journal of Energy and Environmental Engineering*, **9**, 323-339. https://doi.org/10.1007/s40095-018-0271-y

[19] Li, Z., Spaulding, M.L. and French-McCay, D. (2017) An Algorithm for Modeling Entrainment and Naturally and Chemically Dispersed Oil Droplet Size Distribution under Surface Breaking Wave Conditions. *Marine Pollution Bulletin*, **119**, 145-152. https://doi.org/10.1016/j.marpolbul.2017.03.048

[20] Serra, T., Granata, T., Colomer, J., Stips, A., Møhlenberg, F. and Casamitjana, X. (2003) The Role of Advection and Turbulent Mixing in the Vertical Distribution of Phytoplankton. *Estuarine, Coastal and Shelf Science*, **56**, 53-62. https://doi.org/10.1016/s0272-7714(02)00120-8

[21] Tkalich, P. and Chan, E.S. (2002) Vertical Mixing of Oil Droplets by Breaking Waves. *Marine Pollution Bulletin*, **44**, 1219-1229. https://doi.org/10.1016/s0025-326x(02)00178-9

[22] Azevedo, A., Oliveira, A., Fortunato, A.B., Zhang, J. and Baptista, A.M. (2014) A Cross-Scale Numerical Modeling System for Management Support of Oil Spill Accidents. *Marine Pollution Bulletin*, **80**, 132-147. https://doi.org/10.1016/j.marpolbul.2014.01.028

[23] Hole, L.R., Dagestad, K., Röhrs, J., Wettre, C., Kourafalou, V.H., Androulidakis, Y., *et al.* (2019) The Deepwater Horizon Oil Slick: Simulations of River Front Effects and Oil Droplet Size Distribution. *Journal of Marine Science and Engineering*, **7**, Article 329. https://doi.org/10.3390/jmse7100329

[24] Lehr, W., Jones, R., Evans, M., Simecek-Beatty, D. and Overstreet, R. (2002) Revisions of the ADIOS Oil Spill Model. *Environmental Modelling & Software*, **17**, 189-197. https://doi.org/10.1016/s1364-8152(01)00064-0

[25] Copernicus Marine Service (2025) Global Ocean Hourly Sea Surface Wind and Stress from Scatterometer and Model. E.U. Copernicus Marine Service Information (CMEMS), Marine Data Store (MDS). https://doi.org/10.48670/moi-00305

[26] Copernicus Marine Service (2025) Global Ocean Physics Analysis and Forecast. E.U. Copernicus Marine Service Information (CMEMS), Marine Data Store (MDS). https://doi.org/10.48670/moi-00016

[27] Copernicus Marine Service (2025) Global Ocean Waves Analysis and Forecast. E.U. Copernicus Marine Service Information (CMEMS), Marine Data Store (MDS). https://doi.org/10.48670/moi-00017

[28] Breivik, Ø., Bidlot, J. and Janssen, P.A.E.M. (2016) A Stokes Drift Approximation Based on the Phillips Spectrum. *Ocean Modelling*, **100**, 49-56. https://doi.org/10.1016/j.ocemod.2016.01.005

[29] Lamarre, E. and Melville, W.K. (1991) Air Entrainment and Dissipation in Breaking Waves. *Nature*, **351**, 469-472. https://doi.org/10.1038/351469a0

[30] Keramea, P., Kokkos, N., Gikas, G. and Sylaios, G. (2022) Operational Modeling of North Aegean Oil Spills Forced by Real-Time Met-Ocean Forecasts. *Journal of Marine Science and Engineering*, **10**, Article 411. https://doi.org/10.3390/jmse10030411

[31] Röhrs, J., Dagestad, K., Asbjørnsen, H., Nordam, T., Skancke, J., Jones, C.E., *et al.* (2018) The Effect of Vertical Mixing on the Horizontal Drift of Oil Spills. *Ocean Science*, **14**, 1581-1601. https://doi.org/10.5194/os-14-1581-2018

[32] Liu, R., Boufadel, M.C., Zhao, L., Nedwed, T., Lee, K., Marcotte, G., *et al.* (2022) Oil Droplet Formation and Vertical Transport in the Upper Ocean. *Marine Pollution Bulletin*, **176**, Article ID: 113451. https://doi.org/10.1016/j.marpolbul.2022.113451

[33] Johansen, Ø. (2003) Development and Verification of Deep-Water Blowout Models. *Marine Pollution Bulletin*, **47**, 360-368. https://doi.org/10.1016/s0025-326x(03)00202-9

[34] Johansen, Ø., Reed, M. and Bodsberg, N.R. (2015) Natural Dispersion Revisited. *Marine Pollution Bulletin*, **93**, 20-26. https://doi.org/10.1016/j.marpolbul.2015.02.026

[35] Delvigne, G.A.L. and Sweeney, C.E. (1988) Natural Dispersion of Oil. *Oil and Chemical Pollution*, **4**, 281-310. https://doi.org/10.1016/s0269-8579(88)80003-0

[36] Visser, A. (1997) Using Random Walk Models to Simulate the Vertical Distribution of Particles in a Turbulent Water Column. *Marine Ecology Progress Series*, **158**, 275-281. https://doi.org/10.3354/meps158275

[37] Wang, C., Han, L., Zhang, Y., Jiang, A., Wang, J. and Niu, X. (2023) Effects of Physical

Properties and Environmental Conditions on the Natural Dispersion of Oil. *Journal of Marine Science and Engineering*, **12**, Article 47. https://doi.org/10.3390/jmse12010047

[38] Stiver, W. and Mackay, D. (1984) Evaporation Rate of Spills of Hydrocarbons and Petroleum Mixtures. *Environmental Science & Technology*, **18**, 834-840. https://doi.org/10.1021/es00129a006

[39] Jones, R.K. (1997) A Simplified Pseudo-Component Oil Evaporation Model.: *Proceedings of the* 20*th Arctic and Marine Oil Spill Program Technical Seminar*, Vancouver, 11-13 Jun 1997, 43-61. https://inis.iaea.org/search/search.aspx?orig_q=RN:29000027

[40] Devis Morales, A., Rodríguez Rubio, E. and Rincón Martínez, D. (2022) Numerical Modeling of Oil Spills in the Gulf of Morrosquillo, Colombian Caribbean. *CT&F—Ciencia, Tecnología y Futuro*, **12**, 69-83. https://doi.org/10.29047/01225383.396

[41] Adcroft, A., Hallberg, R., Dunne, J.P., Samuels, B.L., Galt, J.A., Barker, C.H., *et al.* (2010) Simulations of Underwater Plumes of Dissolved Oil in the Gulf of Mexico. *Geophysical Research Letters*, **37**, L18605. https://doi.org/10.1029/2010gl044689

[42] Wing, O.E.J., Bates, P.D., Sampson, C.C., Smith, A.M., Johnson, K.A. and Erickson, T.A. (2017) Validation of a 30 M Resolution Flood Hazard Model of the Conterminous United States. *Water Resources Research*, **53**, 7968-7986. https://doi.org/10.1002/2017wr020917

[43] Dearden, C., Culmer, T. and Brooke, R. (2022) Performance Measures for Validation of Oil Spill Dispersion Models Based on Satellite and Coastal Data. *IEEE Journal of Oceanic Engineering*, **47**, 126-140. https://doi.org/10.1109/joe.2021.3099562

[44] Keramea, P., Kokkos, N., Zodiatis, G., Sylaios, G., Coppini, G., Peña, J., *et al.* (2023) Satellite Imagery in Evaluating Oil Spill Modelling Scenarios for the Syrian Oil Spill Crisis, Summer 2021. *Frontiers in Marine Science*, **10**, Article 1264261. https://doi.org/10.3389/fmars.2023.1264261

[45] Brekke, C. and Solberg, A.H.S. (2005) Oil Spill Detection by Satellite Remote Sensing. *Remote Sensing of Environment*, **95**, 1-13. https://doi.org/10.1016/j.rse.2004.11.015